

# Bank of Extended Kalman Filters for Faults Diagnosis in Wind Turbine Doubly Fed Induction Generator

Imane Idrissi<sup>\*1</sup>, Houcine Chafouk<sup>2</sup>, Rachid El Bachtiri<sup>3</sup>, Maha Khanfara<sup>4</sup>

<sup>1,3,4</sup>REEPER GROUP, PERE Laboratory, EST, USMBA University, FEZ, Morocco

<sup>1,2</sup>IRSEEM, ESIGELEC, Normandy University/UNIRouen, Rouen, France

<sup>\*</sup>Corresponding author, e-mail: imane.idrissi@usmba.ac.ma, idrissi@esigelec.fr

## Abstract

*In order to increase the efficiency, to ensure availability and to prevent unexpected failures of the doubly fed induction generator (DFIG), widely used in speed variable wind turbine (SVWT), a model based approach is proposed for diagnosing stator and rotor winding and current sensors faults in the generator. In this study, the Extended Kalman Filter (EKF) is used as state and parameter estimation method for this model based diagnosis approach. The generator windings faults and current instruments defects are modelled, detected and isolated with the use of the faults indicators called residuals, which are obtained based on the EKF observer. The mathematical model of DFIG for both healthy and faulty operating conditions is implemented in Matlab/Simulink software. The obtained simulation results demonstrate the effectiveness of the proposed technique for diagnosis and quantification of the faults under study.*

**Keywords:** extended kalman filter (EKF), doubly fed induction generator (DFIG), speed variable wind turbine (WT), dedicated observer scheme (DOS)

**Copyright © 2018 Universitas Ahmad Dahlan. All rights reserved.**

## 1. Introduction

The wind power generation industry is excitingly growing around the world. According to Global Wind Energy Council (GWEC) statistics, the global cumulative installed wind capacity has developed from 23.900 MW in 2001 to 539.581 MW in 2017. During the last 15 years, doubly fed induction generators (DFIGs) are the most used generators in variable speed wind turbines. The extensively applied configuration of this wind turbine technology is formed of a wound rotor generator with a stator winding connected directly to the grid, while the rotor is coupled to the grid through two power converters, which are rotor-side converter (RSC) and grid-side converter (GSC) [1]. This architecture allows the wind turbine operating in variable speed range, which is approximately -40 to 30% around the synchronous speed and the power electronic converters are conceived to transit only 30% of the nominal generator capacity [2], which makes this configuration attractive and economically interesting.

As all electrical machines, these generators are subjected to diverse types of faults, among which components and sensors faults. The need of an accurate and effective fault detection procedure at the incipient stage is highly required to reduce the operation and maintenance cost of wind energy systems, also to avoid the breakdowns and major damages. When sensors are affected by faults, they provide a wrong image of the physical measured quantities. Therefore the improvement of their reliability seems interesting. Fault detection and isolation in sensors of induction machines has been highlighted in [3, 4, 5]. Moreover, to detect such faults, a Fault diagnosis model based method using an unknown input of multiple observers described via Takagi-Sugeno (T-S) is proposed in [6, 7] proposes a new detection and estimation approach for current sensor faults in the stator and rotor of a DFIG. Furthermore, a robust model-based approach, based on Bond-Graph (BG) theory is proposed in [8] to detect and isolate sensor faults in Doubly Fed Induction Generator (DFIG) wind generators in presence of parameter and sensor measurement uncertainties.

The component faults occurred mainly in the rotor, stator and machine bearing, such as Inter-Turn Short Circuit (ITSC), which happens between two wires within one phase due to insulation deterioration and as the Increased Phase Resistance (IPR) in the rotor and stator windings, slip ring degradation and bearing faults, according to [9]. The ITSC and IPR are the most common defects of DFIG generator and cause an electrical unbalance in the stator and

rotor windings [10]. Only, The IPR fault of both stator and rotor winding of DFIG is tackled in this paper. Model based Detection and Isolation (FDI) methods of parameters faults in induction machines, using estimation techniques have been extensively investigated in the literature. The estimation of parameters using observers or filtering approaches is an indirect procedure, which consists of augmenting the state vector by defining the monitored parameters as additional state variables and the parameters faults are detected through evaluating deviation in the parameters values from their predefined norms. For instance, In order to estimate both the state and the unknown inputs of the DFIG, an unknown input observer (UIO) is used in [11]. The extended kalman filter is used for electrical parameter estimation of doubly-fed induction generators (DFIGs) in variable speed wind turbine systems (WTS) in [12]. An augmented EKF is used to estimate the rotor and stator resistance of the induction motor (IM) drive in [13]. Moreover, the Extended Kalman Filter (EKF) and the Unscented Kalman Filter (UKF) are used for parameter estimation of the doubly fed induction generator (DFIG) driven by wind turbine in [14]. Also, An Extender Kalman Filter-Based Induction Machines Faults Detection is proposed in [15] and the parameter used for the diagnosis is the estimated rotor resistance. Dual EKF is applied also to both state and parameter estimation of vehicle in [16].

To deal the problem of multiple and simultaneous faults detection and localization, the use of a bank of Kalman filters is mainly interesting, this bank can be designed according to a dedicated observer scheme (DOS) as in [17] or structured using a generalized observer scheme (GOS) such as in [18]. In this paper, a bank of EKF structured using the dedicated observer scheme is used for sensor and parameter faults detection and isolation of DFIG's wind turbine. The level of faults is also determined by the investigated approach. In this view, the paper is ordered as follows: In the second section, the non linear state space model of DFIG is established. The third section is about the description of the Extended Kalman filter algorithm and its application for sensors and parameters estimation, more precisely stator and rotor resistances of DFIG system. The fourth section is devoted to the Model-based diagnosis approach of instruments and parameters faults for DFIG system. In the fifth section, the simulation results are presented and discussed. Finally, the conclusion is in the sixth section.

## 2. The Non Linear State Space Model of DFIG

To track changes and to diagnose faults in current sensors and the stator and rotor per phase resistances of the dfig, the state and parameter estimation method used here is based on the Extended Kalman Filter (EKF). The EKF state and parameter estimation requires considering the studied parameters as states and constructing an augmented state vector. As a result, the augmented model is non linear because of multiplication of states. Therefore, the discrete nonlinear state space model of the doubly fed induction generator has been developed in this paragraph. The zero order hold (ZOH) method is used for the model discretization and the sampling time is chosen according to the Shannon theorem. The sixth-order augmented discrete model of DFIG in the two-axis stationary reference frame linked to the rotating magnetic field, named concordia and noted  $(\alpha, \beta)$ , is given by:

$$\begin{cases} x(k+1) = f(x(k), u(k)) + w(k) \\ y(k) = h(x(k), u(k)) + v(k), x(0) = x_0 \end{cases} \quad (1)$$

Where  $w(k)$  and  $v(k)$  are respectively the process and the measurement noises, which are characterized by:

$$\begin{cases} E\{w(k)\} = 0 \\ E\{w(k) \cdot w(k)^T\} = Q \end{cases}, \quad Q \geq 0 \quad (2)$$

$$\begin{cases} E\{v(k)\} = 0 \\ E\{v(k) \cdot v(k)^T\} = R \end{cases}, \quad R \geq 0 \quad (3)$$

$x(k)$  is the state vector formed of the four currents expressed in the concordia reference frame, noted respectively  $i_{s\alpha}$ ,  $i_{s\beta}$ ,  $i_{r\alpha}$  et  $i_{r\beta}$  and of the stator and rotor resistances of dfig, noted respectively  $R_s$  and  $R_r$ .  $y(k)$  is the output vector, formed of the four currents.  $u(k)$  is the input

vector composed of the stator and rotor voltages of the generator in the stationary reference frame, noted respectively  $v_{s\alpha}$ ,  $v_{s\beta}$ ,  $v_{r\alpha}$ ,  $v_{r\beta}$ . The state vector is expressed as follows:

$$\begin{aligned} x(k) &= [x_1(k) \ x_2(k) \ x_3(k) \ x_4(k) \ x_5(k) \ x_6(k)]^T \\ x(k) &= [i_{s\alpha}(k) \ i_{s\beta}(k) \ i_{r\alpha}(k) \ i_{r\beta}(k) \ R_s(k) \ R_r(k)]^T \end{aligned} \quad (4)$$

The input vector is given by:

$$\begin{aligned} u(k) &= [u_1(k) \ u_2(k) \ u_3(k) \ u_4(k)]^T \\ u(k) &= [v_{s\alpha}(k) \ v_{s\beta}(k) \ v_{r\alpha}(k) \ v_{r\beta}(k)]^T \end{aligned} \quad (5)$$

The discrete state space model of dfig in detailed form is given by the set of the following (6) to (9):

$$\begin{aligned} x_1(k+1) &= -\frac{1}{\sigma \cdot L_s} \cdot x_5(k) \cdot x_1(k) + \left(\frac{1-\sigma}{\sigma} \cdot \omega + \omega_s\right) \cdot x_2(k) + \frac{M}{\sigma \cdot L_s \cdot L_r} \cdot x_6(k) \cdot x_3(k) \\ &+ \frac{M}{\sigma \cdot L_s} \cdot \omega \cdot x_4(k) + \frac{1}{\sigma \cdot L_s} \cdot u_1(k) - \frac{M}{\sigma \cdot L_s \cdot L_r} \cdot u_3(k) + w_1(k) \end{aligned} \quad (6)$$

$$\begin{aligned} x_2(k+1) &= -\left(\frac{1-\sigma}{\sigma} \cdot \omega + \omega_s\right) \cdot x_1(k) - \frac{1}{\sigma \cdot L_s} \cdot x_5(k) \cdot x_2(k) + \frac{M}{\sigma \cdot L_s} \cdot \omega \cdot x_3(k) \\ &+ \frac{M}{\sigma \cdot L_s \cdot L_r} \cdot x_6(k) \cdot x_4(k) + \frac{1}{\sigma \cdot L_s} \cdot u_1(k) - \frac{M}{\sigma \cdot L_s \cdot L_r} \cdot u_3(k) + w_2(k) \end{aligned} \quad (7)$$

$$\begin{aligned} x_3(k+1) &= \frac{M}{\sigma \cdot L_s \cdot L_r} \cdot x_5(k) \cdot x_1(k) - \frac{M}{\sigma \cdot L_r} \cdot \omega \cdot x_2(k) - \frac{1}{\sigma \cdot L_r} \cdot x_6(k) \cdot x_3(k) \\ &+ \left(\omega_s - \frac{\omega}{\sigma}\right) \cdot x_4(k) - \frac{M}{\sigma \cdot L_s \cdot L_r} \cdot u_1(k) + \frac{1}{\sigma \cdot L_r} \cdot u_3(k) + w_3(k) \end{aligned} \quad (8)$$

$$\begin{aligned} x_4(k+1) &= \frac{M}{\sigma \cdot L_r} \cdot \omega \cdot x_1(k) + \frac{M}{\sigma \cdot L_s \cdot L_r} \cdot x_5(k) \cdot x_2(k) - \left(\omega_s - \frac{\omega}{\sigma}\right) \cdot x_3(k) \\ &- \frac{1}{\sigma \cdot L_r} \cdot x_6(k) \cdot x_4(k) - \frac{M}{\sigma \cdot L_s \cdot L_r} \cdot u_2(k) + \frac{1}{\sigma \cdot L_r} \cdot u_4(k) + w_4(k) \end{aligned} \quad (9)$$

In this study the DFIG per phase resistances are supposed to be constant during the time of simulation; therefore, the state space equations are given by:

$$x_5(k+1) = x_5(k) + w_5(k) \quad (10)$$

$$x_6(k+1) = x_6(k) + w_6(k) \quad (11)$$

where  $R_s$ ,  $R_r$ ,  $L_s$ ,  $L_r$  and  $M$  are respectively stator per phase resistance, rotor per phase resistance, cyclic stator and rotor and mutual inductances.  $\omega_s$  is the synchronism angular speed [ $rad \cdot s^{-1}$ ],  $\omega$  is the mechanical angular speed [ $rad \cdot s^{-1}$ ] and it is given by:

$$\omega = \omega_s - \omega_r = p \cdot \Omega_{mec} \quad (12)$$

where  $\Omega_{mec}$  is the mechanical speed of DFIG [ $rpm$ ],  $p$  is the poles number and  $\omega_r$  is the rotor angular speed [ $rad \cdot s^{-1}$ ],  $\sigma = 1 - \frac{M^2}{L_s \cdot L_r}$  is the leakage coefficient. Terms  $w_1(k)$ ,  $w_2(k)$ ,  $w_3(k)$ ,  $w_4(k)$ ,  $w_5(k)$  and  $w_6(k)$  are the zero mean process noises.

### 3. Extended Kalman Filter (EKF)

The classical kalman filter was originally in 1960 by the mathematician, electrical engineer and inventor Rudolf Emil Kalman. Its main advantage is the ability to provide estimates of system states, outputs and parameters, which are not directly measurable by physic sensors

or which are prone to statistical noises and other inaccuracies. This concept is widely applied for navigation and vehicles control as aircraft and spacecraft. Furthermore, it is used in fields such as signal processing, economic and widely for estimation and tracking. The recursive filter kalman algorithm consists of two successive steps that are: firstly the prediction step of the actual state of a system based on its inputs, followed by the correction stage in which the state estimations, previously made, are updated using available and measurable system outputs. Basically, the Standard Kalman filter (SKF) was devoted to the estimation of the non-measurable states of linear systems. In fact, most of physical systems have a non linear behavior, hence a powerful extension called extended Kalman filter (EKF), has been developed for state and parameter estimation of non-linear systems, which requires a linearization at each working point of the state equations.

$$\hat{x}[0] = \hat{x}_0 = E\{x_0\} \quad (13)$$

$$P_0 = P[0] = E\{(x_0 - \hat{x}[0])(x_0 - \hat{x}[0])^T\} \quad (14)$$

$$K_0 = K[0] = P[0] \cdot H[0]^T \cdot (H[0] \cdot P[0] \cdot H[0]^T + R)^{-1} \quad (15)$$

The second step aims to predict the system state  $\hat{x}_{k|k-1}$  and its error covariance matrix  $P_{k|k-1}$  starting from the previous state estimate  $\hat{x}_{k-1|k-1}$  and the input vector  $u_{k-1}$ .

$$\hat{x}_{k|k-1} = \hat{x}_{k-1|k-1} + f(x_{k-1|k-1}, U_{k-1}) + w_{k-1} \quad (16)$$

$$P_{k|k-1} = P_{k-1|k-1} + F_{k-1} \cdot P_{k-1|k-1} \cdot F_{k-1}^T + Q_{k-1} \quad (17)$$

Where  $Q_{k-1}$  is the process error covariance matrix and  $F_{k-1}$  is the system gradient matrix (discrete Jacobian matrix), given by:

$$F_{k-1} = \frac{\partial f}{\partial x}|_{x = \hat{x}_{k-1|k-1}} \quad (18)$$

In the third step, the local observability of the considered system should be verified. For  $k \geq 1$ , we have:

$$n_k = n[k] = \text{rank}(O_{\text{bsv}}[k]) \quad (19)$$

With  $O_{\text{bsv}}[k]$  is the observability matrix defined as in (24).

The fourth stage performs a correction of the predicted state estimate  $\hat{x}_{k|k}$  and its estimation error covariance matrix  $P_{k|k}$  using the system measured quantities. Formally, we have:

$$K_k = P_{k|k-1} \cdot H_k^T \cdot (H_k \cdot P_{k|k-1} \cdot H_k^T + R_k)^{-1} \quad (20)$$

$$\hat{x}_{k|k} = \hat{x}_{k|k-1} + k_k \cdot [z_k - h(\hat{x}_{k|k-1})] \quad (21)$$

$$P_{k|k} = (I - K_k \cdot H_k) \cdot P_{k|k-1} \quad (22)$$

Where  $K_k$  is the optimal kalman gain,  $R_k$  is the measurement error covariance matrix,  $z_k$  are the system measurement quantities and  $H_k$  is the Jacobian matrix expressed as:

$$H_k = \frac{\partial h}{\partial x}|_{x = \hat{x}_{k|k-1}} \quad (23)$$

The choice of the matrices  $P_0$ ,  $Q$  and  $R$  represent a critical point in the design of the EKF, because that affects the EKF convergence and its estimation performance.

### 3.2. Application of the EKF for DFIG Currents and Resistances Estimation

The application of the observer (EKF) for the currents and resistances estimation of the generator dfig requires firstly the system observability verification. Since the dfig model is a nonlinear system, the observability of the linearized model should be verified locally around each operating point [21]. The observability can be verified by calculating the observability matrix and its rank, the observability matrix of the linearized model of dfig is given by:

$$O_{bsv}[K] = [H_k \quad H_k \cdot F_k \quad H_k \cdot F_k^2 \quad H_k \cdot F_k^3 \quad H_k \cdot F_k^4 \quad H_k \cdot F_k^5]^T \quad (24)$$

The pair  $\{F[k], H[k]\}$  is observable if and only if the observability matrix  $O_{bsv}[k]$  has full rank, that's to say, for dfig model,  $rank(O_{bsv}[K]) = 6$ , where six represent the number of the dfig model states.  $F_k$ ,  $H_k$  and  $O_{bsv}[k]$  are calculated for each sampling instant  $k \geq 0$ .

The Jacobian matrix of the system state  $F_k$ , the input matrix  $B_k$  and the observation matrix  $H_k$  are computed and expressed in the order mentioned as follows:

$$F_k = \begin{bmatrix} -a_1 & a \cdot \omega + \omega_s & a_3 & a_5 \cdot \omega & 0 & 0 \\ -(a \cdot \omega + \omega_s) & -a_1 & -a_5 & a_3 & 0 & 0 \\ a_4 & -a_6 \cdot \omega & -a_2 & \left(\omega_s - \frac{\omega}{\sigma}\right) & 0 & 0 \\ a_6 \cdot \omega & a_4 & -\left(\omega_s - \frac{\omega}{\sigma}\right) & -a_2 & 0 & 0 \\ 0 & 0 & 0 & 0 & a_7 & 0 \\ 0 & 0 & 0 & 0 & 0 & a_8 \end{bmatrix} \quad (25)$$

where  $a = \frac{1-\sigma}{\sigma}$ ,  $a_1 = \frac{a_7}{\sigma \cdot L_s}$ ,  $a_2 = \frac{a_8}{\sigma \cdot L_r}$ ,  $a_3 = \frac{a_8 \cdot M}{\sigma \cdot L_s \cdot L_r}$ ,  $a_4 = \frac{a_7 \cdot M}{\sigma \cdot L_s \cdot L_r}$ ,  $a_5 = \frac{M}{\sigma \cdot L_s}$ ,  $a_6 = \frac{M}{\sigma \cdot L_r}$ ,  $a_7 = R_s$ ,  $a_8 = R_r$

the input matrix  $B_k$

$$B_k = \begin{bmatrix} b_1 & 0 & -b_3 & 0 & 0 & 0 \\ 0 & b_1 & 0 & -b_3 & 0 & 0 \\ -b_3 & 0 & b_2 & 0 & 0 & 0 \\ 0 & -b_3 & 0 & b_2 & 0 & 0 \\ 0 & 0 & 0 & 0 & 0 & 0 \\ 0 & 0 & 0 & 0 & 0 & 0 \end{bmatrix} \quad (26)$$

where  $b_1 = \frac{1}{\sigma \cdot L_s}$ ,  $b_2 = \frac{1}{\sigma \cdot L_r}$ ,  $b_3 = \frac{M}{\sigma \cdot L_s \cdot L_r}$

the output or observation matrix  $H_k$

$$H_k = \begin{bmatrix} 1 & 0 & 0 & 0 & 0 & 0 \\ 0 & 1 & 0 & 0 & 0 & 0 \\ 0 & 0 & 1 & 0 & 0 & 0 \\ 0 & 0 & 0 & 1 & 0 & 0 \\ 0 & 0 & 0 & 0 & 1 & 0 \\ 0 & 0 & 0 & 0 & 0 & 1 \end{bmatrix} \quad (27)$$

$P_0$  is the initial error covariance matrix,  $Q$  is the noise covariance matrix and  $R$  is the error covariance matrix. In general, the covariance matrices  $P_0$ ,  $Q$  and  $R$  are assumed to be diagonal matrices because of the insufficient statistical information to evaluate their off-diagonal terms.

## 4. Model-based Diagnosis Approach of Instruments and Parameters Faults for DFIG System

### 4.1. Design of the Model-based Fault Diagnosis Procedure for DFIG System

Model-based fault diagnosis in a system consists of comparing the available measurement quantities with the information provided by the mathematical model of the system. This procedure is known as analytical redundancy, which is cost effective and reliable than the hardware redundancy. According to the literature, fault diagnosis procedure can be summarized in three main tasks, which are: - Fault detection aims to decide if the system is in good condition or not, - Fault isolation step allows determining the location of the fault and the fault evaluation

enables the estimation of the fault level and its type or nature. Faults can be classified according to their location to three types, which are sensor, actuator or process faults. In this paper, the current sensors and resistances faults in additive form are studied, but the adopted approach can be extended to other forms of faults such as multiplicative and other nonlinear functions.

The proposed FDI procedure comprises two main stages, which are the system mathematical modeling, residual generation and decision making. The first stage is presented in the section 2 entitled "State space model of dfig". The residual generation aims to generate fault indicator signals by means of the input and output of the monitored system. The residual signal generated should be independent of the system operating state and takes into account only the fault condition. When no fault occurs, the residual signal should be a zero-mean or close to zero-mean noise sequence, however, it is different from zero-mean once the fault is present. The means used for the residuals generation is called a residual generator. The residuals are obtained by comparing the sensory measurements to analytical values calculated by the EKF observer.

#### 4.2. Design of the Model-based Fault Diagnosis Procedure for DFIG system

Despite being known as a strong machine, DFIG is never far from failures. These anomalies lead to abnormal behavior of the generator and can cause its total damage in short or long term. Doubly fed induction generators are strongly prone to sensor faults and to the parameters faults. One of the most common faults of resistances in induction machines is that the increased phase resistance (IPR) in the rotor and stator windings. This defect is essentially caused by the excessive increase of the windings temperature. Moreover, the DFIG rotor asymmetry has been reported to be a significant indicator of generator faults. Taking into account their occurrence frequency and their negative effect on the machine normal operation, the current instruments faults, the IPR fault of stator windings and the electrical asymmetry defect of the DFIG, are modeled and diagnosed. Several scenarios are established and the adopted FDI procedure has been applied. In order to simulate several faults situations as in reality, the fault modeling step is needed.

a. Current sensors faults modeling: sensor faults affect instruments and can be expressed mathematically as an additive term as follows:

$$y(t) = y_R(t) + f_s(t) \quad (28)$$

where  $y(t)$  is the measured output vector,  $y_R(t)$  is the system output vector.  $f_s(t)$  represents the sensor fault vector.

b. Increased stator phase resistance fault model: This component fault affects the per phase resistances of DFIG and leads to an increase in the resistance value due to the increasing temperature. It can be mathematically modeled by[21]:

$$R = R_0 \cdot (1 + \alpha \cdot \Delta T) \quad (29)$$

where  $R$  is the per-phase resistance,  $R_0$  is the stator per phase resistance at the temperature  $T_0 = 25 \text{ }^\circ\text{C}$ ,  $\Delta T$  is the temperature variation and  $\alpha$  is the temperature coefficient respectively of the stator (copper) and rotor (copper or aluminum) windings.  $\alpha_{Cu} = 3,93 \cdot 10^{-3} \text{ }^\circ\text{C}^{-1}$  and  $\alpha_{Al} = 4,03 \cdot 10^{-3} \text{ }^\circ\text{C}^{-1}$

c. Rotor electrical asymmetry modeling

The rotor electrical asymmetry fault is caused by the open circuit in one or more of rotor windings or in the circuits of gear-brush and also by the increased value of rotor resistance. This fault doesn't cause rapidly the fail of the generator, but it can lower the generator reliability and efficiency, that's why it should be avoided. Rotor electrical asymmetries can be modelled by adding an external variable resistance, denoted  $R_{ex}$  in series with the rotor phase windings. When,  $R_{ex}$  has a value greater than zero, the faulted phase resistance occurred [22]. The asymmetrical resistance of the rotor is given as a percentage of the balanced phase rotor resistance, with the rotor asymmetry,  $\Delta R$ , as a percentage, is:

$$\Delta R_r = \frac{R_{ex}}{R_r} \times 100 \quad (30)$$

where  $R_r$  is the resistance of the rotor phase winding under normal operation, the values of  $R_{ex}$  and  $\Delta R_r$  are relative to the severity degree of the imbalance.

**4.3. Bank of Extended Kalman Filters Design for FDI**

In order to achieve the detection and localization of multiple and simultaneous faulty sensors or resistances of DFIG system, a bank of Extended Kalman observers approach is designed. Each observer is directed by one element of the system measurement vector  $y$  and the input vector  $u$ , and produces an output estimate  $\hat{y}$  and parameter estimate vector  $\hat{\theta}$ . Also, the appropriate residual signals, which are the difference between the measurement and the predicted measurement from the EKF, are generated. Each kalman filter is designed under normal condition and sensitive to a particular fault. In this study, the FDI system is structured according to the dedicated observer scheme (DOS), in which the number of observers is equal to the number of sensors and each observer is provided all the system inputs and just one output. So the supervised system must be observable through each of the instruments, that is to say, the state of DFIG is observable through each of the six outputs and each pair  $\{F, H_i\}$  for  $(i=1, 2, 3, 4,5,6)$  the system is observable. Where  $H$  is the output matrix or the observation matrix, and can be written in the following form:

$$H = [H_1^T \quad H_2^T \quad H_3^T \quad H_4^T \quad H_5^T \quad H_6^T] \tag{31}$$

The following Figure 1 shows the FDI system structure for DFIG with the dedicated observer scheme.

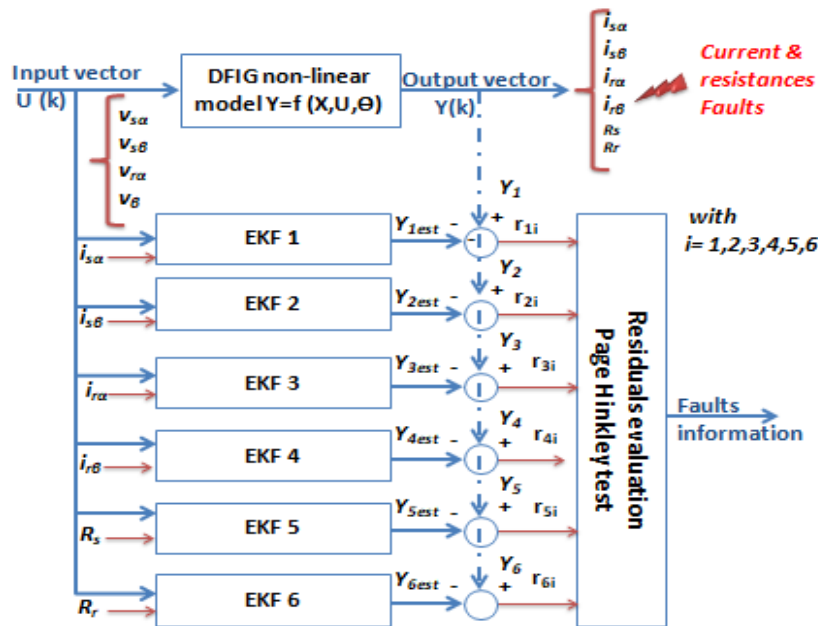


Figure 1. The FDI system structure according to the DOS scheme

where  $Y_{1est}$ ,  $Y_{2est}$ ,  $Y_{3est}$ ,  $Y_{4est}$ ,  $Y_{5est}$  and  $Y_{6est}$  are the outputs estimates provided by each extended kalman observer.

**5. Simulation Results**

The variable speed wind turbine model based on DFIG with a power of 3 Kw has been developed and simulated using MATLAB / Simulink software. The turbine and DFIG parameters are extracted from [23]. The random wind velocity applied to the model of wind turbine, is presented in Figure 2. Figure 3 shows the variable mechanical speed of the DFIG.

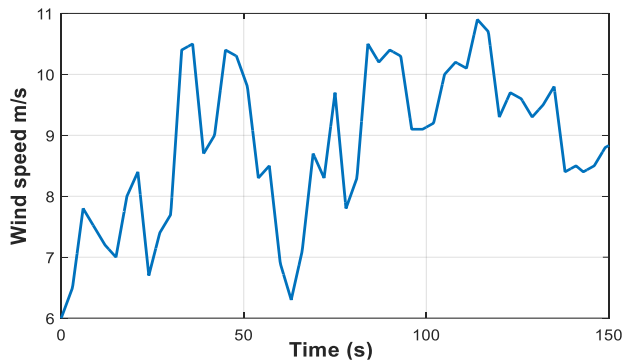


Figure 2. The random wind velocity [m·s<sup>-1</sup>]

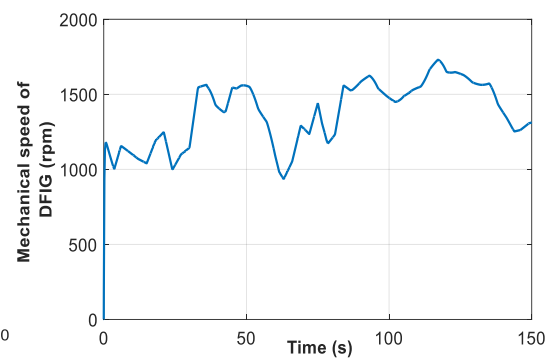


Figure 3. The mechanical speed of the DFIG rotor [rpm]

The stator and rotor currents of the generator expressed in the ( $\alpha$ ,  $\beta$ ) reference frame and under healthy condition, are given respectively in Figure 4.

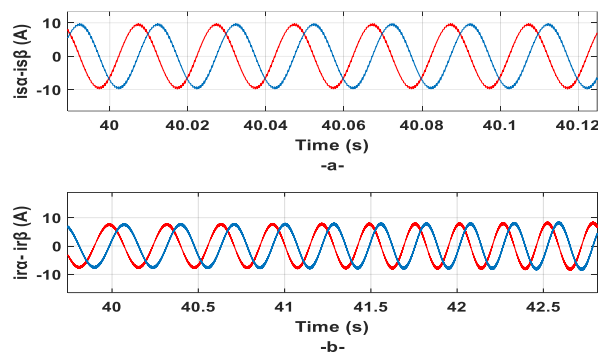


Figure 4. Currents of DFIG in the concordia reference frame (A) -a- Stator currents of DFIG; -b- Rotor currents of DFIG

### 5.1. Currents and Resistances Estimates by a Single EKF for DFIG System

A single EKF can be used to estimate the currents and resistances of the DFIG. The observability condition is verified and the estimation errors of the EKF are shown in Figure 5:

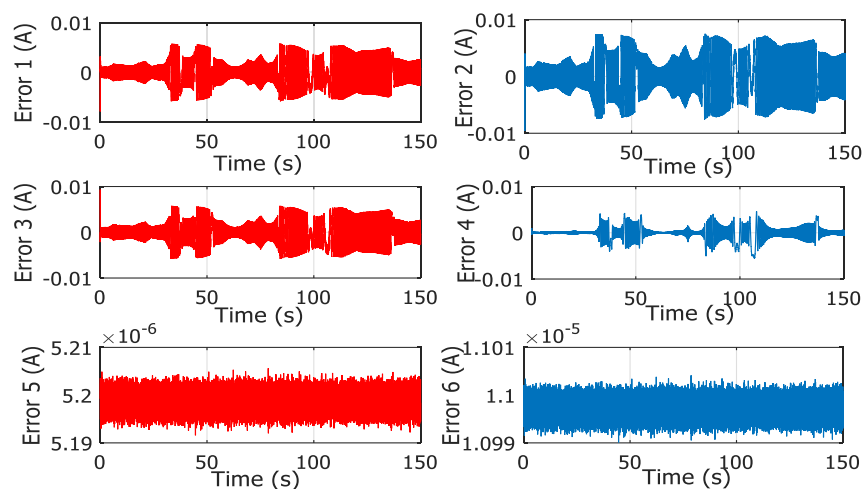


Figure 5. The estimation errors of the DFIG outputs using the single EKF

The estimation errors of the EKF are obtained by means of comparing the system measurements provided by the non linear model of DFIG and their estimates given by the single EKF. Error 1, Error 2, Error 3, Error 4, Error 5 and Error 6 are respectively the estimation errors of the currents  $i_{s\alpha}$ ,  $i_{s\beta}$ ,  $i_{r\alpha}$ ,  $i_{r\beta}$  and the per phase stator resistance  $R_s$  and the per phase rotor resistance  $R_r$ . These estimation errors are equal to very small values, which show that the EKF is a good and performant estimator.

**5.2. Resistances Faults and their Impact on the System State**

**5.2.1. Increased phase resistance (IPR) of the stator generator:**

Considering at first the following defect scenario: an increase of 10%, 20%, 30% and 40% around the nominal value of the stator phase resistance was applied successively and was injected at time ( $t= 0s$ ). the figures below indicate the temporal variation of the mechanical velocity of the generator, the stator current in the axis  $\alpha$  and the rotor current in the axis  $\beta$  under both the healthy and faulty conditions.

Figure 6 and Figure 7 indicate that the mechanical velocity of DFIG is sensitive to this type of fault. The mechanical velocity amplitude decreases with each increase in the value of the stator resistance. The stator current remains almost unchanged in the presence of defects as shown in Figure 8 and the rotor current is unbalanced because there is a slight phase difference between the healthy operation and the malfunctions. Therefore, it can be deduced that the state variables which are the rotor current and mechanical velocity of DFIG are variables that produce more information about the behavior of the generator in the presence of this type of defect. Figure 9 shows rotor current in the axis  $\beta$  in the different cases of the IPR defect

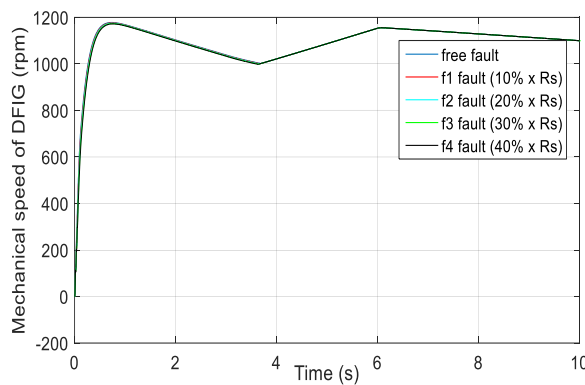


Figure 6. The mechanical velocity of the generator DFIG under the different IPR defect

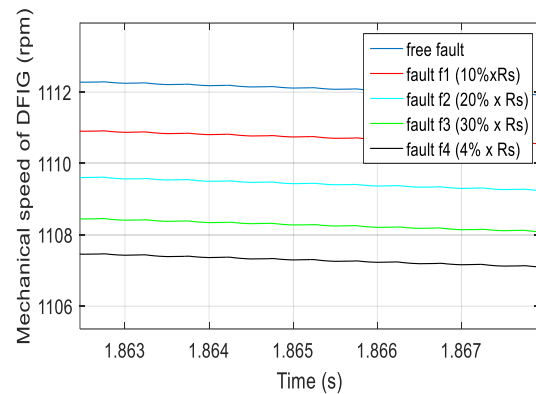


Figure 7. Zoom of the mechanical velocity amplitudes variation

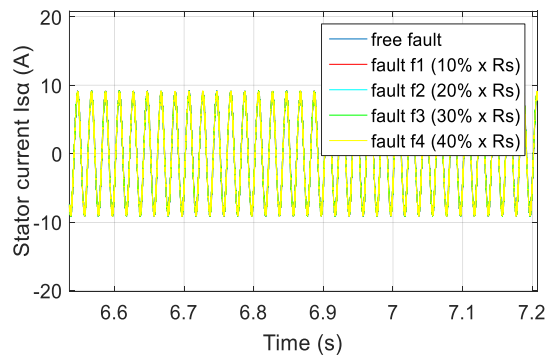


Figure 8. Stator current in the axis  $\alpha$  in the different cases of the IPR defect

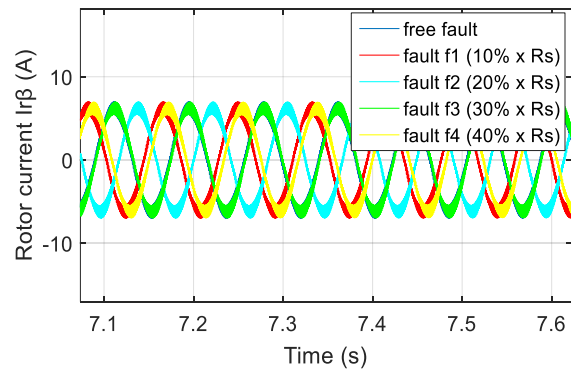


Figure 9. Rotor current in the axis  $\beta$  in the different cases of the IPR defect

### 5.2.2. Rotor Electrical Asymmetry Fault and its Effect on the System State

The rotor per phase resistance is about  $2.2 \Omega$  and an additional resistance has a value of  $0.22 \Omega$  is successively added to a phase which causes the rotor electrical asymmetry of: 10%, 20%, 40% and 60%. This fault is injected at time ( $t=0s$ ). The impact of this type of fault on the state variables of the studied system, which are the stator and rotor currents, the rotor angular speed of the generator, is presented in the following Figures 10-12:

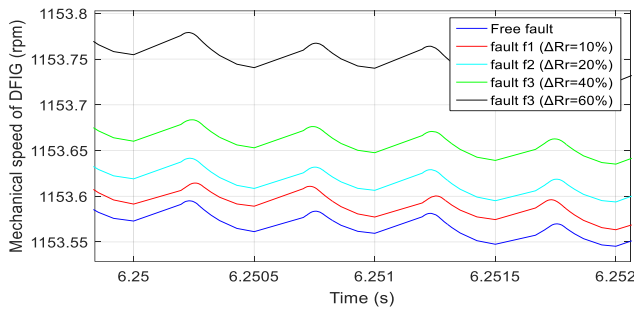


Figure 10. Zoom of the angular velocity amplitudes variation under the rotor electrical asymmetry defect

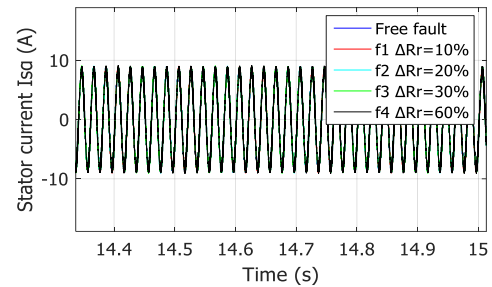


Figure 11. The stator current  $i_{s\alpha}$  (A) under the rotor electrical asymmetry defect cases

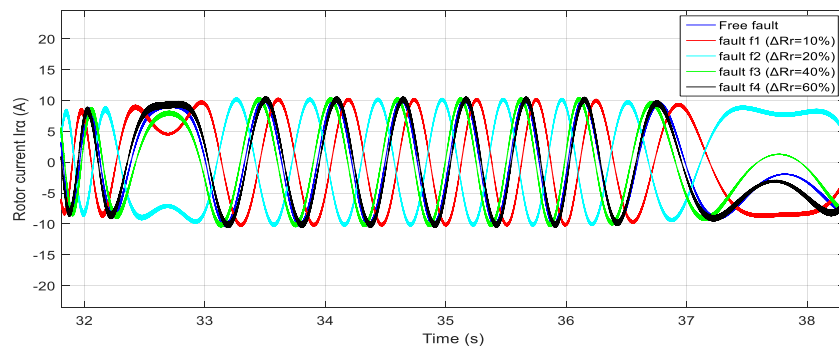


Figure 12. The rotor current  $i_{r\alpha}$  (A) under the rotor electrical asymmetry defect

It can be observed that this type of defect influences the mechanical velocity. Figure.10 shows a variation of the mechanical velocity amplitude for the four fault cases. The angular velocity increases with each increase of the  $\Delta R_r$  value. The same remark as before can be made for the stator currents, which are unchanged when the fault occurred, however, the rotor current are getting unbalanced between the healthy operation and the faulty cases. Therefore, it can be deduced that the state variables, which are the rotor currents and the rotor angular velocity are variables that produce more information about the behavior of the generator in the presence of this type of defect.

### 5.3. Residuals Generation

Considering, an increased stator phase resistance and a rotor electrical asymmetry fault are applied as the scenarios summarized in the two following tables and the obtained residuals are shown in Figure 13.

The second scenario consists of introducing an additive fault in the first current sensor which measures the current  $i_{s\alpha}$  and the previous faulty scenario of resistances is reproduced. This sensor fault started at  $t=5s$  and disappeared at  $t=7s$  and it is an offset with a constant amplitude equal to 6 A. The obtained residual signals, generated by the single EKF block are given in the Figure 14. The Scenario of Stator Resistance IPR fault as shown in Table 2 and the scenario of the rotor electrical asymmetry defect as shown in Table 3.

From Figure 13, we can notice that the residual signals 5 and 6 confirm the presence of the faults aforementioned, while, the other residuals 1, 2, 3 and 4 are varying around zero, which prove that the four current sensors are not faulty. Figure 14 shows that is difficult to localize exactly the faulty current sensor or the faulty resistance. Therefore, the dedicated kalman filters scheme is used to deal with this fault localization problem. Using the multiple model extended kalman filters structured according to the dedicated observer scheme (DOS), we obtained the results presented in the set of these figures:

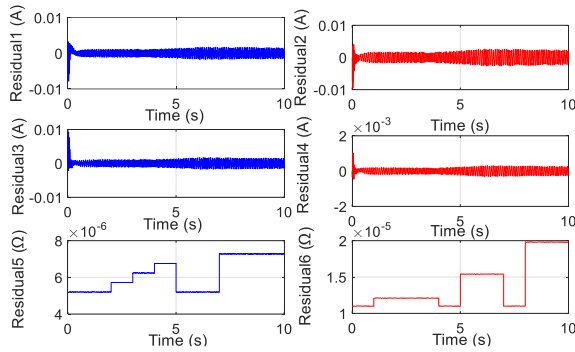


Figure 13. Residual signals for the fault scenario 1

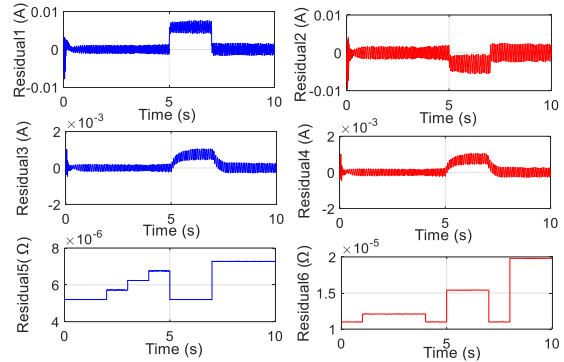


Figure 14. Residual signals for the fault scenario 2

Table 2. The Scenario of Stator Resistance IPR Fault

period	$\Delta R_s$
2st-3s	10% x $R_s$
3s-4s	20% x $R_s$
4s- 5s	30% x $R_s$
7s-10s	40% x $R_s$

Table 3. The Scenario of the Rotor Electrical Asymmetry Defect

period	$\Delta R_r$ (%)
1s-4s	10
5s-7s	40
8s-10s	60

The residuals generated by the extended kalman observer 1, 5 and 6 directed by The faulty outputs, don't allow us to localize exactly the faulty sensor or resistance. Moreover, the three Extended kalman observers, directed by the faultless outputs, generate the set of residual signals shown in Figures 15-20. Through the redundant results given by these signals, we can localize the faulty sensor and parameters, which are the current sensor 1 and the two resistances  $R_s$  and  $R_r$ . Also, the level of the faults can be deduced.

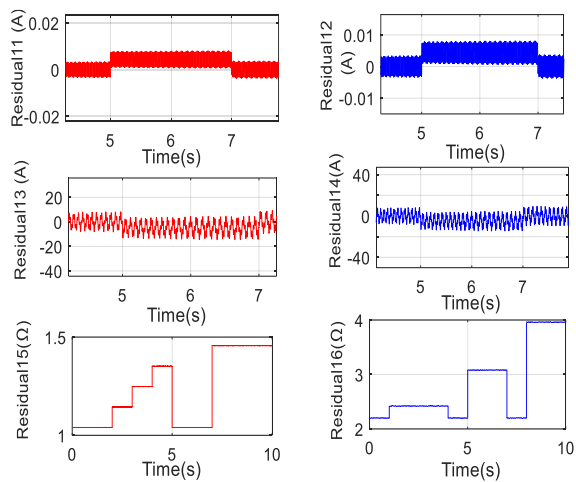


Figure 15. Residuals of the extended kalman observer 1

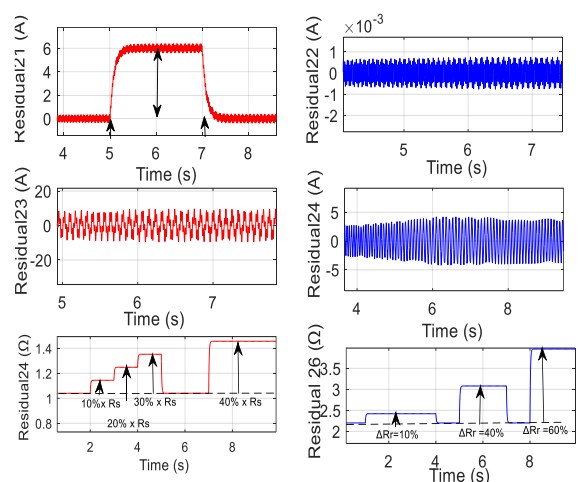


Figure 16. Residuals of the extended kalman observer 2

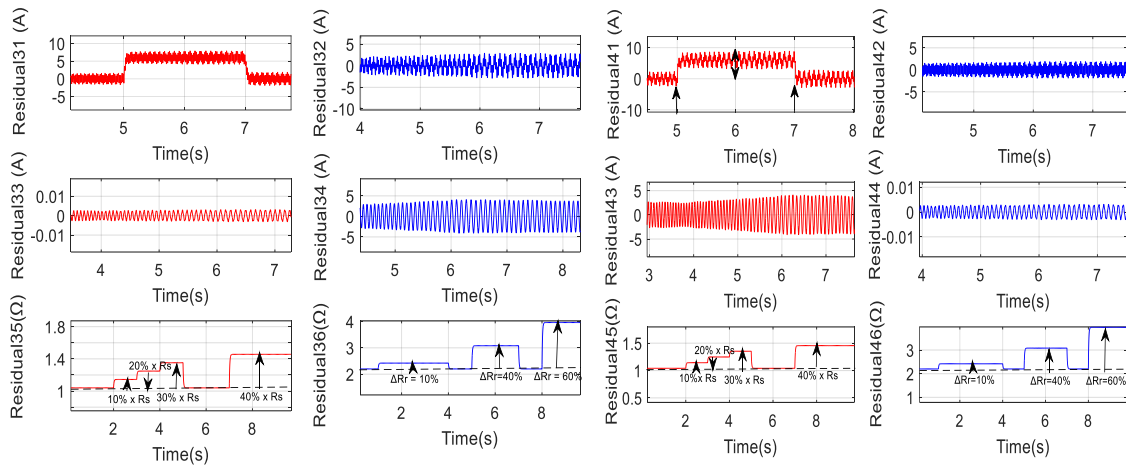


Figure 17. Residuals of the extended kalman observer 3

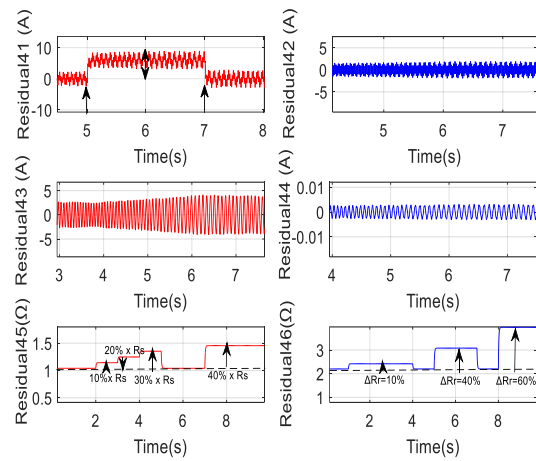


Figure 18. Residuals of the extended kalman observer 4

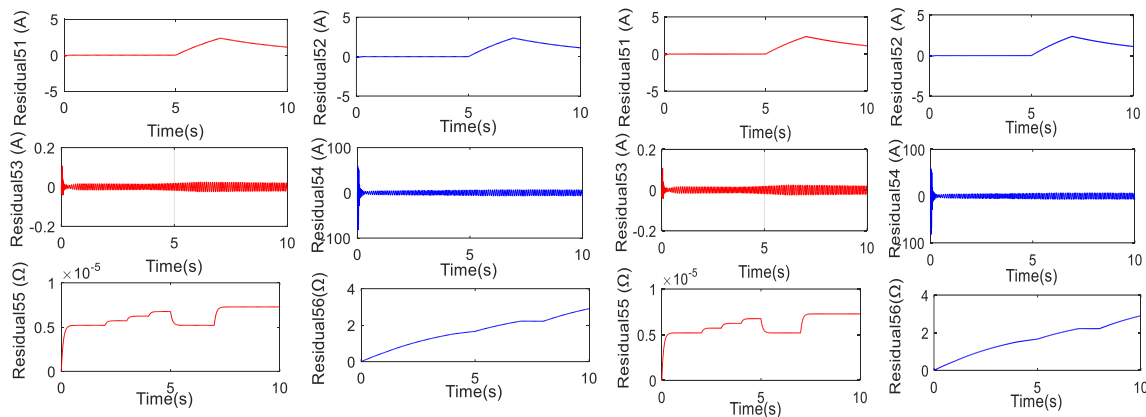


Figure 19. Residuals of the extended kalman observer 5

Figure 20. Residuals of the extended kalman observer 6

## 6. Conclusion

This paper treats the problem of fault detection and isolation (FDI) in the current sensors and resistances of DFIG. The effect of these faults on the system state variables, which are rotor current and angular velocity, has been shown. To detect and isolate one current sensor fault, a single extended kalman filter is used. To deal with multiple faults, the multiple model extended kalman filters structured according to the dedicated observer scheme (DOS) has been designed.

## References

- [1] R Arindya. A Variable Speed Wind Generation System Based on Doubly Fed Induction Generator. *Bulletin of Electrical Engineering and Informatics (BEEI)*. 2013; 2(4): 272-277.
- [2] T Ackermann. *Wind Power in Power Systems*. 2005: 745.
- [3] R Saravanakumar, M Manimozhi, DP Kothari, et M Tejenosh. Simulation of Sensor Fault Diagnosis for Wind Turbine Generators DFIG and PMSM Using Kalman Filter. *Energy Procedia*. 2014; 54: 494-505.
- [4] H Li, C Yang, YG Hu, B Zhao, M Zhao, et Z Chen. Fault-tolerant control for current sensors of doubly fed induction generators based on an improved fault detection method. *Measurement*. January 2014; 47: 929-937.

- [5] GHB Foo, XZhang, et DM Vilathgamuwa. A Sensor Fault Detection and Isolation Method in Interior Permanent-Magnet Synchronous Motor Drives Based on an Extended Kalman Filter. *IEEE Trans. Ind. Electron.* August 2013; 60(8): 3485-3495.
- [6] H Chafouk et H Ouyessaad. Fault Detection and Isolation in DFIG Driven by a Wind Turbine. *IFAC-Pap.* 2015; 48(21): 251-256.
- [7] Abdelmalek Samir, Rezazi Sarah, et Azar, Ahmad Taher. Sensor Faults Detection and Estimation for a Dfig Equipped Wind Turbine. *Energy Procedia.* 2017; 139: 3-9.
- [8] A Mojallal et S Lotfifard. DFIG Wind Generators Fault Diagnosis Considering Parameter and Measurement Uncertainties. *IEEE Trans. Sustain. Energy.* April 2018; 9(2): 792-804.
- [9] Y Amirat, M Benbouzid, B Bensaker, et R Wamkeue. Condition Monitoring and Fault Diagnosis in Wind Energy Conversion Systems: A Review. 2007 IEEE International Electric Machines & Drives Conference. 3-5 May 2007.
- [10] S Abdelmalek, L Barazane, et A Larabi. Unknown Input Observer for a Doubly Fed Induction Generator Subject to Disturbances. *International Journal of Power Electronics and Drive Systems (IJPEDS).* December 2015; 6(4), p. 781-787.
- [11] M Abdelrahem, C Hackl, et R Kennel. *Application of extended Kalman filter to parameter estimation of doubly-fed induction generators in variable-speed wind turbine systems.* in International Conference on Clean Electrical Power (ICCEP), Taormina. Italy, 2015: 226-233.
- [12] J Talla, Z Peroutka, V Blahnik, et L Streit. *Rotor and Stator Resistance Estimation of Induction Motor Based on Augmented EKF.* International Conference on Applied Electronics. 8-9 September 2015.
- [13] SP Azad et JE Tate. *Parameter estimation of doubly fed induction generator driven by wind turbine.* in 2011 IEEE/PES Power Systems Conference and Exposition, Phoenix, AZ, USA, 2011: 1-8.
- [14] A Chahmi, M Bendjebbar, B Raison, et M Benbouzid. An Extender Kalman Filter-based Induction Machines Faults Detection. *International Journal of Electrical and Computer Engineering (IJECE).* April 2016; 6(2): 535-548.
- [15] TA Wenzel, KJ Burnham, MV Blundell, et RA Williams. Dual extended Kalman filter for vehicle state and parameter estimation. *Veh. Syst. Dyn.* February 2006; 44(2): 153-171.
- [16] L Li, Z Wang, et Y Shen. *Fault diagnosis for attitude sensors via a bank of extended Kalman filters.* in 35th Chinese Control Conference (CCC), Chengdu, China. 2016: 6634-6638.
- [17] J Zarei et J Poshtan. Sensor Fault Detection and Diagnosis of a Process Using Unknown Input Observer. *Math. Comput. Appl.* April 2011; 16(1): 31-42.
- [18] S Nadarajan, SK Panda, B Bhangu, et AK Gupta. Online Model-Based Condition Monitoring for Brushless Wound-Field Synchronous Generator to Detect and Diagnose Stator Windings Turn-to-Turn Shorts Using Extended Kalman Filter. *IEEE Trans. Ind. Electron.* May 2016; 63(5): 3228-3241.
- [19] S Bolognani, L Tubiana, et M Zigliotto. Extended kalman filter tuning in sensorless PMSM drives. *IEEE Trans. Ind. Appl.* November 2003; 39(6): 1741-1747.
- [20] G Lefebvre, JY Gauthier, A Hijazi, X Lin Shi, et V Le Digarcher. Observability-Index-Based Control Strategy for Induction Machine Sensorless Drive at Low Speed. *IEEE Trans. Ind. Electron.* March 2017; 64(3): 1929-1938.
- [21] JC Trigeassou Éd. *Electrical machines diagnosis.* London: ISTE. 2011.
- [22] M Zaggout, L Ran, P Tavner, et C Crabtree. Detection of rotor electrical asymmetry in wind turbine doubly-fed induction generators. *IET Renew. Power Gener.* November 2014; 8(8): 878-886.
- [23] P Krafczyk. Modélisation et mise en oeuvre d'une chaîne de production éolienne à base de la MADA. 2015.